Chapter 3

Structural and optical properties of Eu doped GaN.

Among rare earth materials, Eu seems to be a most interesting element since red emission which was hard to be achieved by using InGaN system, has now become possible in GaN. The red emission is of critical importance on achieving monolithic full color light emitting devices based on GaN. In this chapter, the structural and optical properties of Eu doped GaN were reviewed and characterized in the view point of feasible application on novel photoelectron device.

3.1 Structural properties of Eu doped GaN.

3.1.1 Surface structure of Eu doped GaN observed by RHEED.

Fig. 3-1 shows the typical RHEED pattern taken along [11$\bar{2}$0] azimuth after partial growth steps of the Eu doped GaN with the Eu cell temperature ranging between 390°C and 500°C. The growth temperature of all Eu doped GaN samples were 700°C. After the growth of undoped GaN with the thickness of 350nm, RHEED pattern was streaky as shown in Fig. 3-1(a) indicating a flat surface with a 2 dimensional growth. The streaky pattern gradually changes to a spotty pattern as the Eu doping is initiated started, indicating the surface roughness enhancement. When the Eu doping concentration is relatively low (for example, 390°C for this case), the pattern changes into a spotty 1×1 shape shown in Fig. 3-1(b) which indicates a 3 dimensional island growth of single crystalline hexagonal structure. The shape maintained through out the whole growth.

When the Eu cell temperature increases up to 450°C the RHEED pattern shows a somewhat different feature from that of Fig. 3-1(b). Fig. 3-1(c) gives the RHEED pattern of Eu doped GaN at an Eu cell temperature of 450°C -the author will call hereafter Eu:GaN_Eu450°C- or higher, with a thickness of about 4nm. The spotty pattern in this figure is different from typical hexagonal diffraction of GaN, and rather closer to the pattern than the typical diffraction pattern of cubic structure of GaN. Upon further growth of Eu:GaN_Eu450°C, the spotty pattern becomes dominant and faint extra spots appear. The RHEED patter, after 2 hour growth, is depicted in Fig. 3-1 (d). A ring pattern as shown in Fig. 3-1 (e), however, was observed after 2hour growth of Eu:GaN with Eu cell temperature of 500°C and this result indicates poly crystalline growth.

The RHEED pattern of Eu:GaN_Eu450°C after 2 hour growth was observed intensively as combined with TEM of which the result will be shown in next section. Fig. 3-2 (a) show closer view of the RHEED pattern. The RHEED pattern was interpreted to be composed of a combination of the streak patter from hexagonal phase of GaN and spots from cubic phase including also extra spots from face and from twin of those spots as shown in Fig. 3-2 (b). The results suggest that Eu doping enhances the 3D-growth mode and spot pattern of cubic phase and typical twin structure, which reveals that Eu doping enhances the stacking fault formation. The time for the change from streaky to spotty pattern depended on Eu cell temperature. That is, the enhancement of the 3D-growth mode and stacking fault formation seem to depend on the Eu concentration.

3.1.2 Micro-graphical structure of Eu:GaN observed by AFM, SEM, TEM.

The AFM micrographs of Eu:GaN with various Eu concentrations are shown in Fig. 3-3. As the Eu cell temperature increased, the surface became rougher and the size of grain increased. The sample grown at the Eu cell temperature of 390°C (Fig. 3-3 (a)) shows a relatively flat surface and smaller grain while 450°C-Eu:GaN sample shows a large hunch and rough surface as shown in Fig. 3-3 (d). The root-mean square (rms) roughness as a function of the reciprocal temperature of the Eu cell was

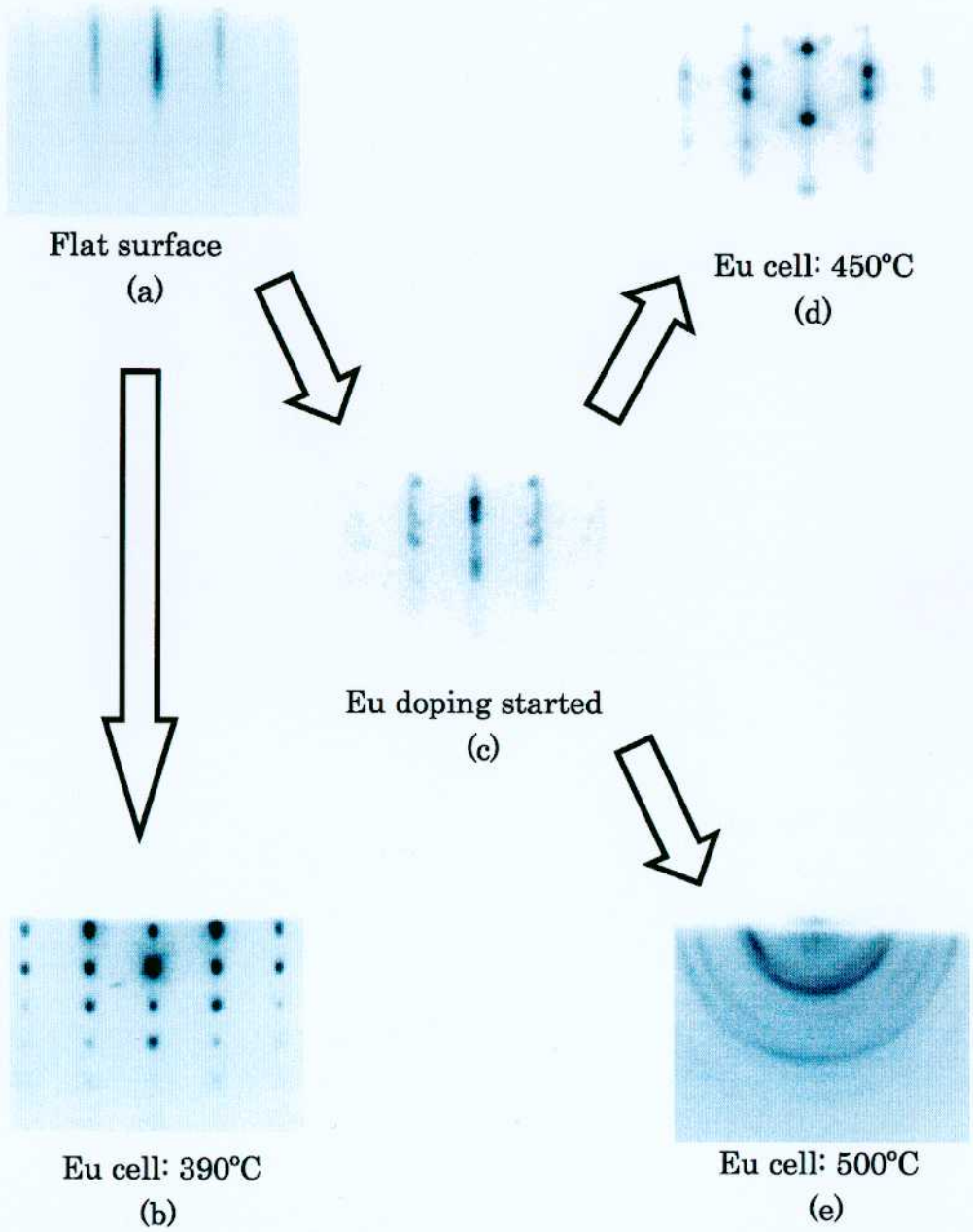

Figure 3-1: RHEED patterns of Eu:GaN at various Eu cell temperatures

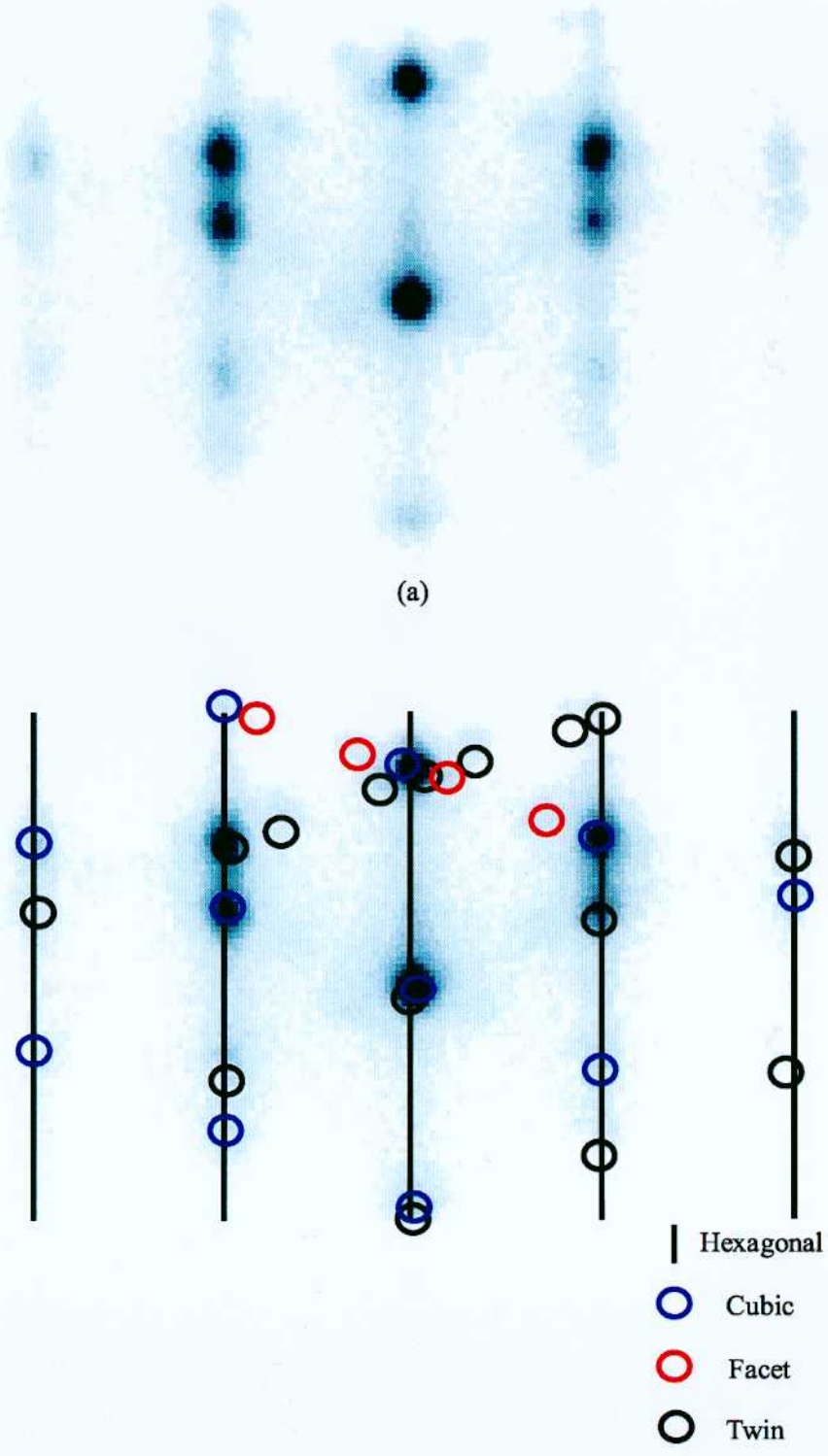

Figure 3-2: (a)RHEED pattern of Eu:GaN after 2 hour growth with Eu cell temperature of 450°C and (b)interpretation of the pattern.

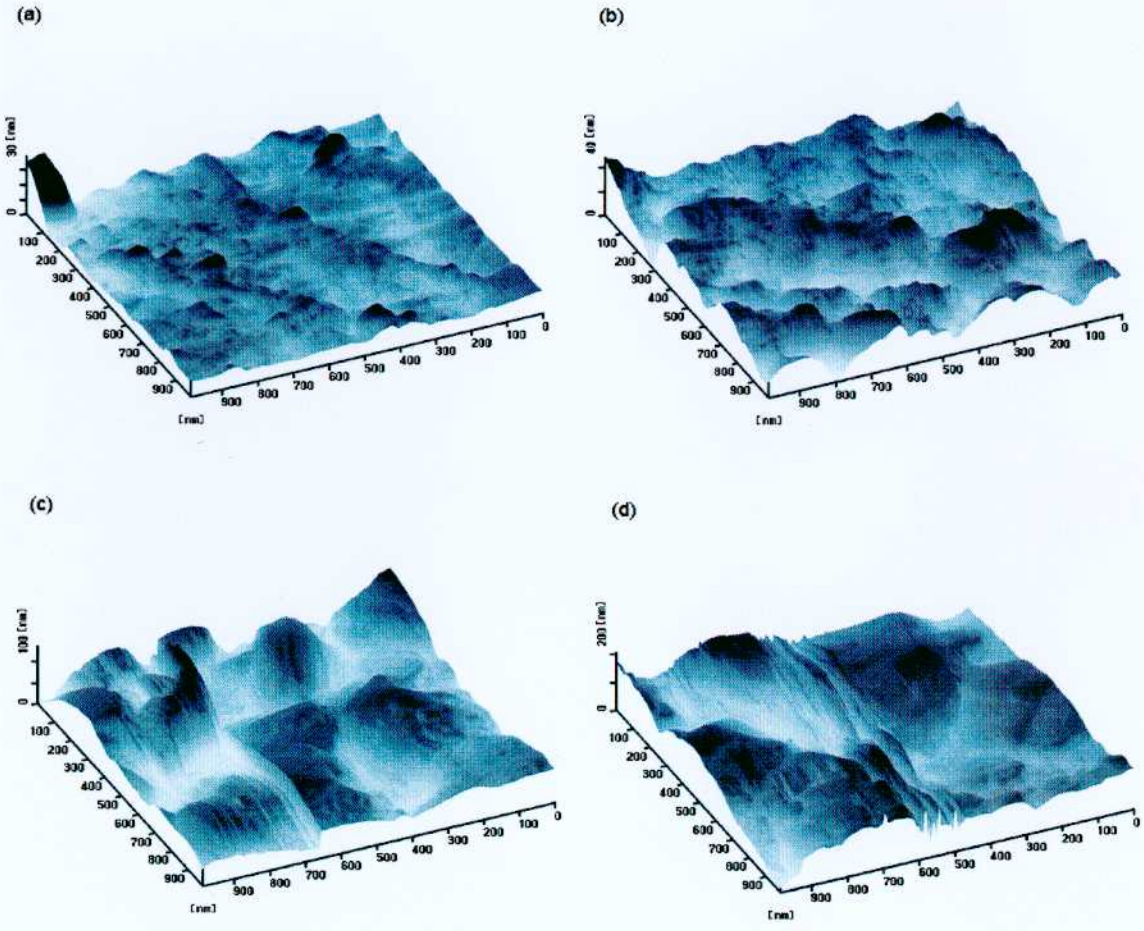

Figure 3-3: AFM micrographs of Eu doped GaN grown with the Eu cell temperature of (a) 390°C, (b) 410°C, (c) 430°C, and (d) 450°C.

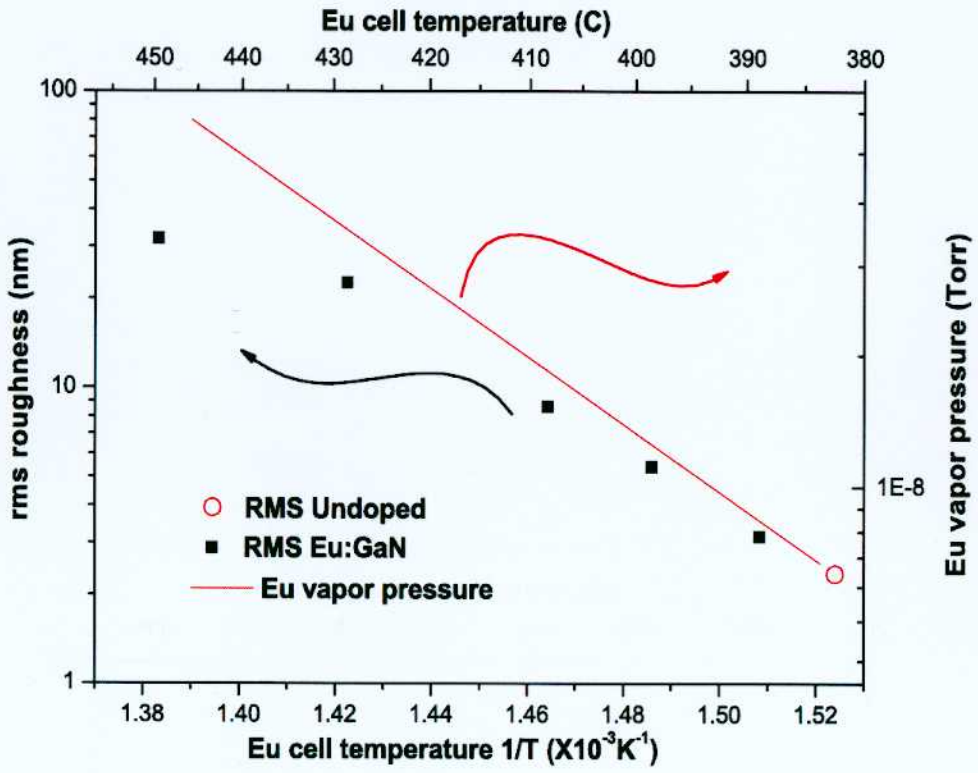

Figure 3-4: RMS roughness of Eu-doped GaN vs. inverse temperature of the Eu cell. The RMS value of undoped GaN and Vapor pressure curve of Eu are shown for reference.

plotted in Fig. 3-4. The vapor pressure curve of Eu was also shown for reference. It is clear that as the temperature of Eu cell increases from 390°C to 450°C, the root-mean square (rms) roughness increases from 3.16 to 32nm. The increase of the rms roughness shows an approximately linear relation with the inverse temperature of the Eu cell in this temperature range and is almost parallel to the vapor pressure curve of Eu. This result suggests that the 3 dimensional -growth character is linearly proportional to the Eu concentration consistent with the RHEED observation.

The 3 dimensional surface structures were confirmed by SEM observation also. The SEM image of Eu:GaN_Eu450°C is shown in Fig. 3-5. From the figure, a clear island shape surface structure was observed and each island seems to have inclined facets. The facets are considered to be the cause of extra spots in RHEED pattern shown in Fig. 3-2.

Fig. 3-6 (a) show a selected area diffraction (SAD) pattern of Eu:GaN. The incident beam direction was normal to $(11\bar{2}0)$ plane of GaN. The plots constitute the patterns are interpreted to be from the diffraction of Hexagonal phase and Cubic phase of GaN and its twins with the symmetric planes of (100) of cubic phase or $(10\bar{1}0)$ of hexagonal phase as shown in Fig. 3-5 (b). These results are consistent with the result of RHEED interpretation. It is now clear that Eu doping with Eu cell temperature higher than 450°C evokes the introduction of cubic phase and twin structure. Clear feature of introduction of cubic phase and twin structure were confirmed by high resolution TEM picture shown in Fig. 3-7.

Eu ion has much bigger covalent radius than that of Ga ion (Eu; 0.185nm, Ga; 0.126nm)[3-1], so the incorporation of Eu ion into Ga lattice site (will be mentioned in section 3.1.4.) is expected to cause lattice strain or distortion. When the Eu doping rate is relatively high, the strain or distortion are relaxed by stacking fault, which results formation of cubic phase, and twins. When the Eu doping rate is relatively low, the strain can be relaxed without introducing those structures as confirmed in RHEED pattern of Eu:GaN_ Eu390°C.

3.1.3 Crystalline qualities studied by XRD.

Fig. 3-8 shows XRD profiles of Eu:GaN with various Eu cell temperatures and undoped GaN. A peak at 2θ=34.60° for sample (b) is just the same as that from the (0002) reflection of undoped GaN. Peak shift to lower angle possibly caused by bigger covalent radius of Eu ion and manifest broadening of full width at half maximum (FWHM) was observed on sample (c). On the other hand, in sample (d), two kinds of materials, GaN and EuN, were detected, that is, a peak at 34.60° can be assigned as (0002) GaN reflection and peak at 36.0° as (200) EuN reflection[3-2]. The peak around 39.5° can be assigned as reflection of (200) of cubic GaN. Comparing the peak intensities of GaN with EuN, most of Eu atoms are considered to form EuN compounds.

Since the θ-2θ mode is not sensitive to asymmetric direction, the structural film qualities for both symmetric and asymmetric directions for the samples with Eu concentration up to 2 at.% (Eu cell temperature 450°C) were compared by ω-2θ mode X-ray diffraction. It was impossible to detect a

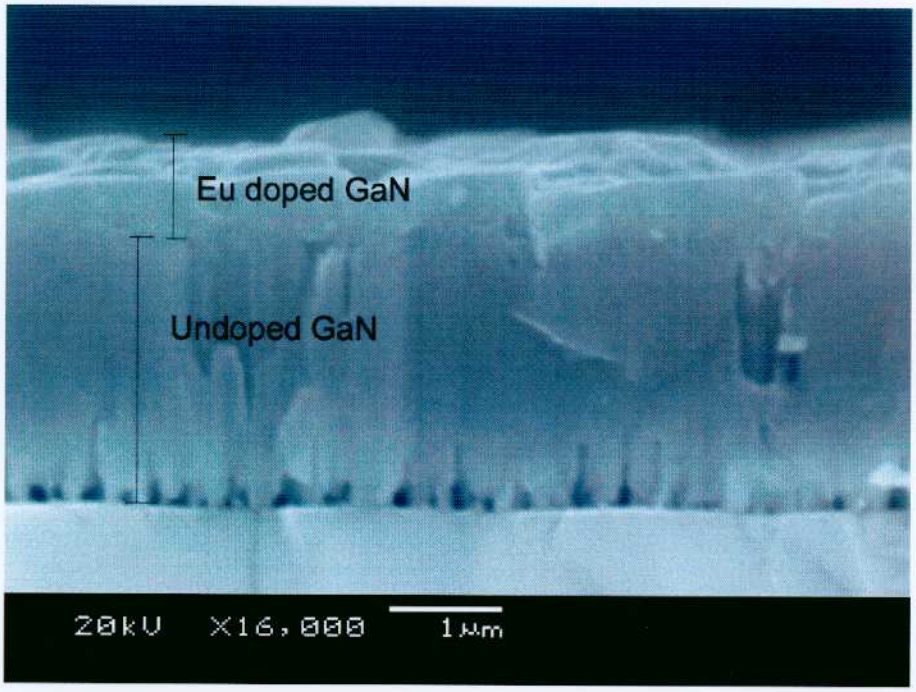

(a)

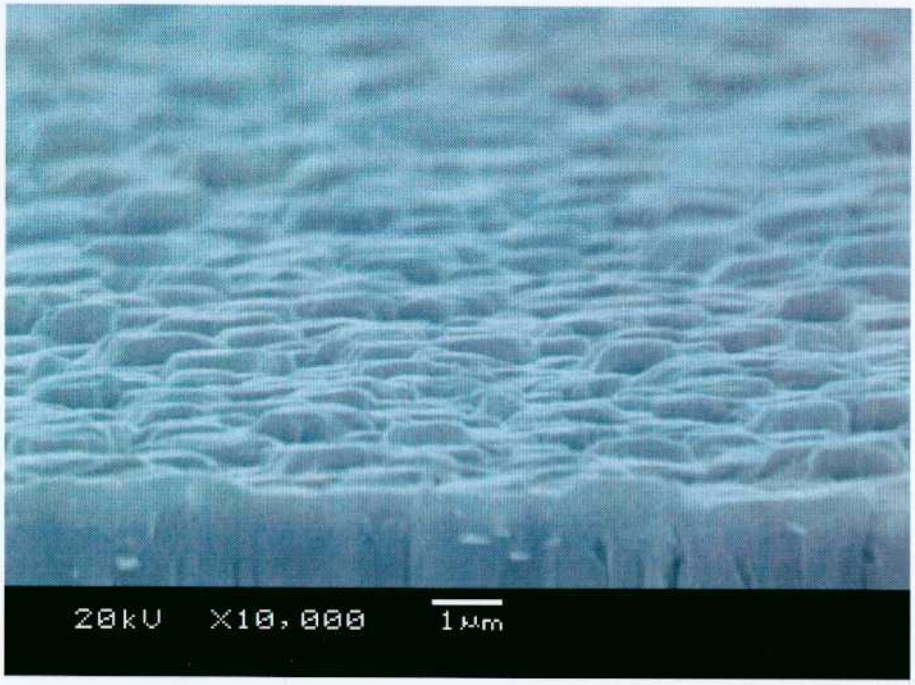

(b)

Figure 3-5: The SEM image of Eu:GaN with Eu cell temperature of 450°C (a) Cross-sectional view (b) 45 degree tilted surface view.

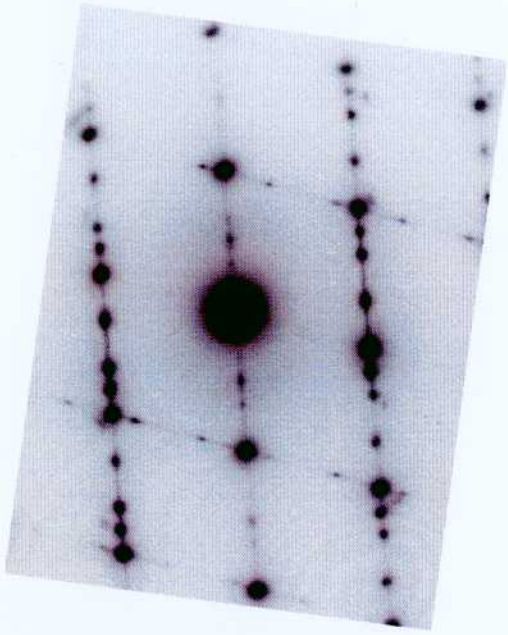

(a)

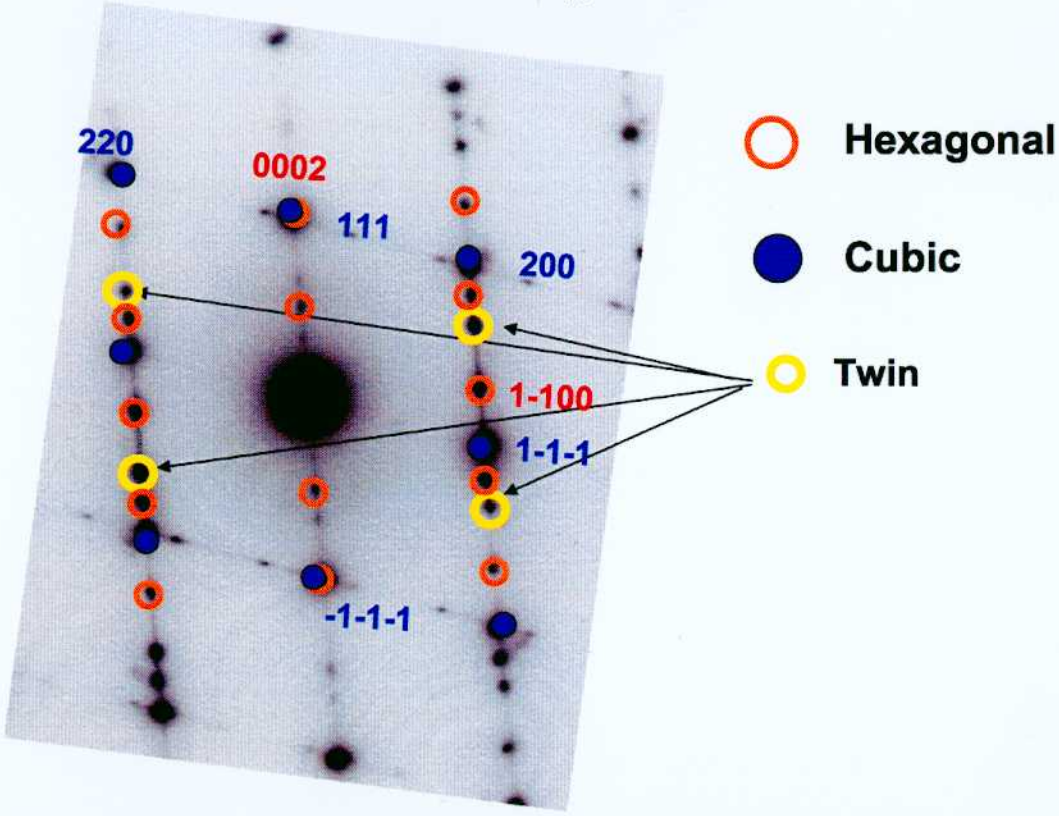

(b)

Figure 3-6: (a) Selected area diffraction of Eu:GaN and (b) its interpretation.

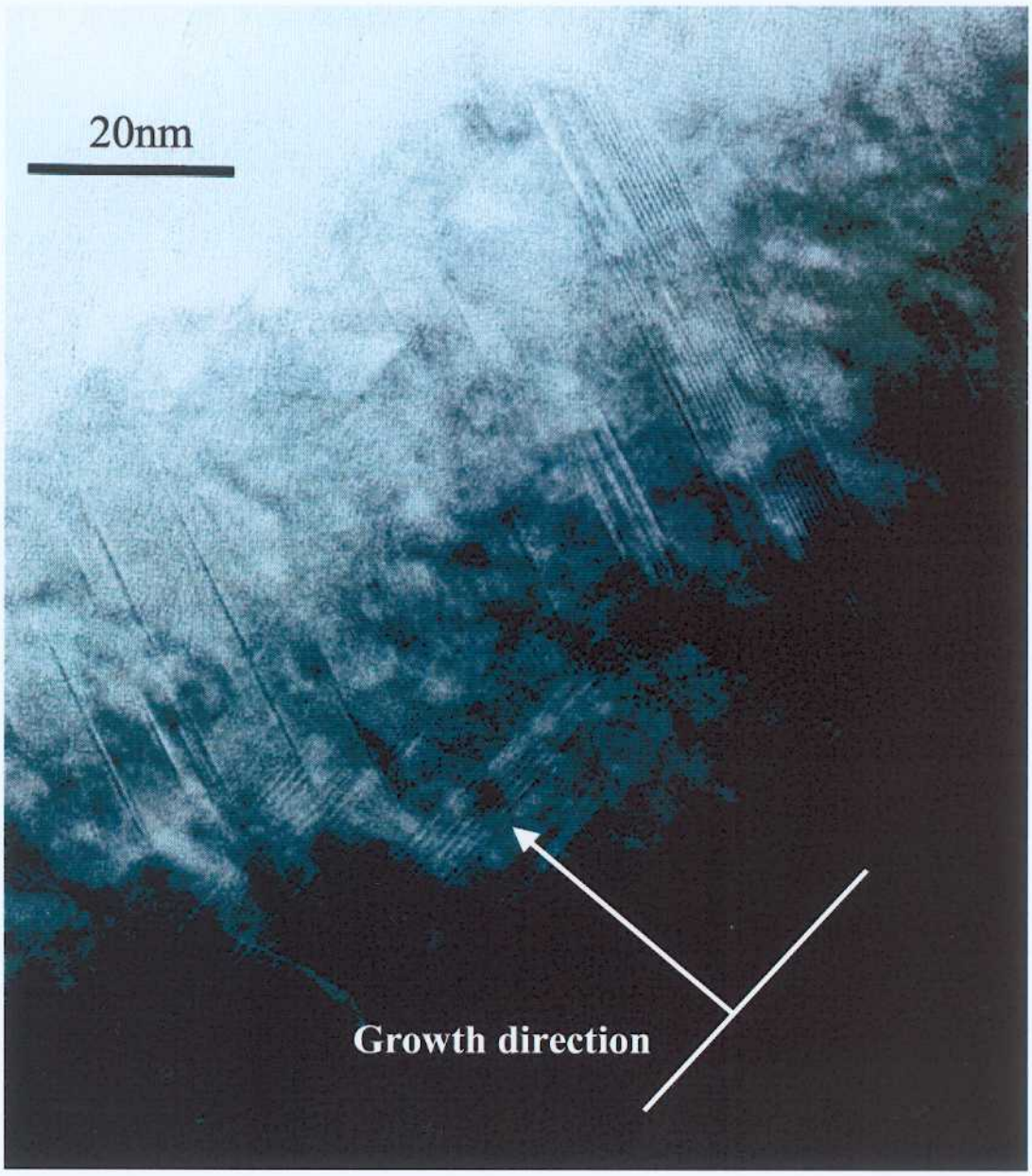

Figure 3-7: High resolution TEM image of Eu:GaN.

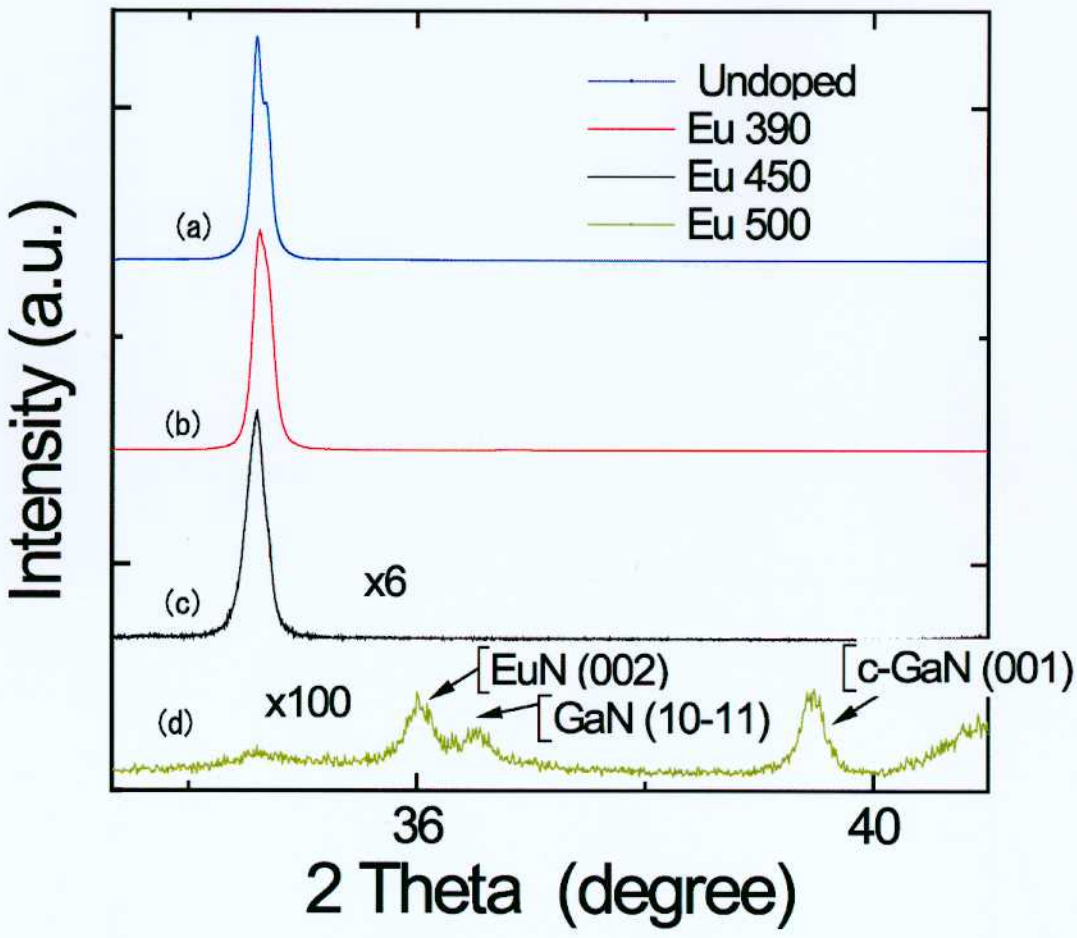

Figure 3-8: X-ray diffraction profile of Eu doped GaN with various Eu cell temperatures (a) undoped, (b) Eu 390°C, (c) Eu 450°C, (d) Eu 500°C.

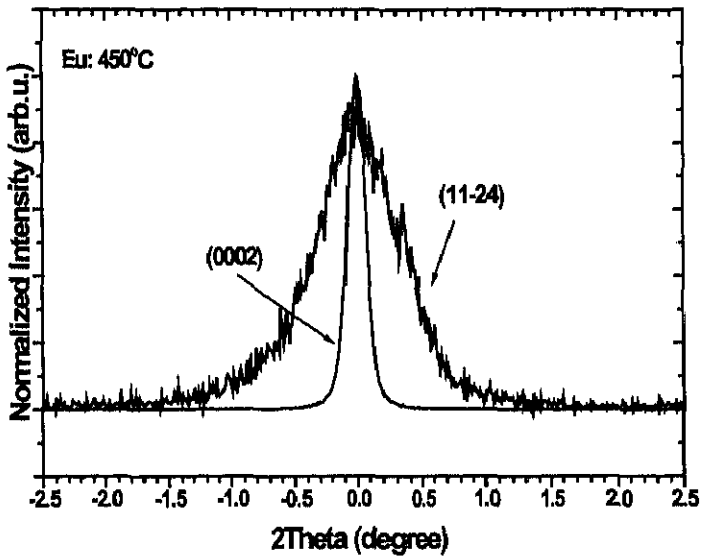

Figure 3-9: Superimposed symmetric and asymmetric ω-2θ X-ray diffraction profiles for Eu doped GaN grown with the Eu cell temperature of 450°C

Table 3-I: The FWHM values of symmetric and asymmetric diffraction from Eu-doped GaN

Eu temp (°C)	390	410	430	450
FWHM (0002) arcsec	422	450	470	539
FWHM ($11\bar{2}4$) arcsec	1833	2001	2276	2620

peak for the sample with higher Eu concentration than 2at.% due to low intensity of signals. Both symmetric (0002) and asymmetric ($11\bar{2}4$) diffraction from Eu:GaN grown with the Eu cell temperature of 450°C are shown in Fig 3-9. The symmetric diffraction showed a much broader FWHM than the symmetric one. The FWHM values of diffraction peaks for Eu:GaN with various Eu concentrations are listed in Table 3-I. It was observed that as the temperature of the Eu cell increases, the FWHM values of both symmetric and asymmetric diffraction peaks increase and the asymmetric diffraction peaks are broadened in a faster way than the symmetric one. In hexagonal GaN, taking account of the relation with the direction of Burgers vector, the FWHM of the symmetric diffraction is sensitive only to screw- and/or mixed-type threading dislocations, while pure edge dislocations in addition to the screw and mixed dislocations contribute to the FWHM of the asymmetric diffraction.

Since the lattice spacing of (111) plane of cubic GaN and (0002) plane of hexagonal GaN is

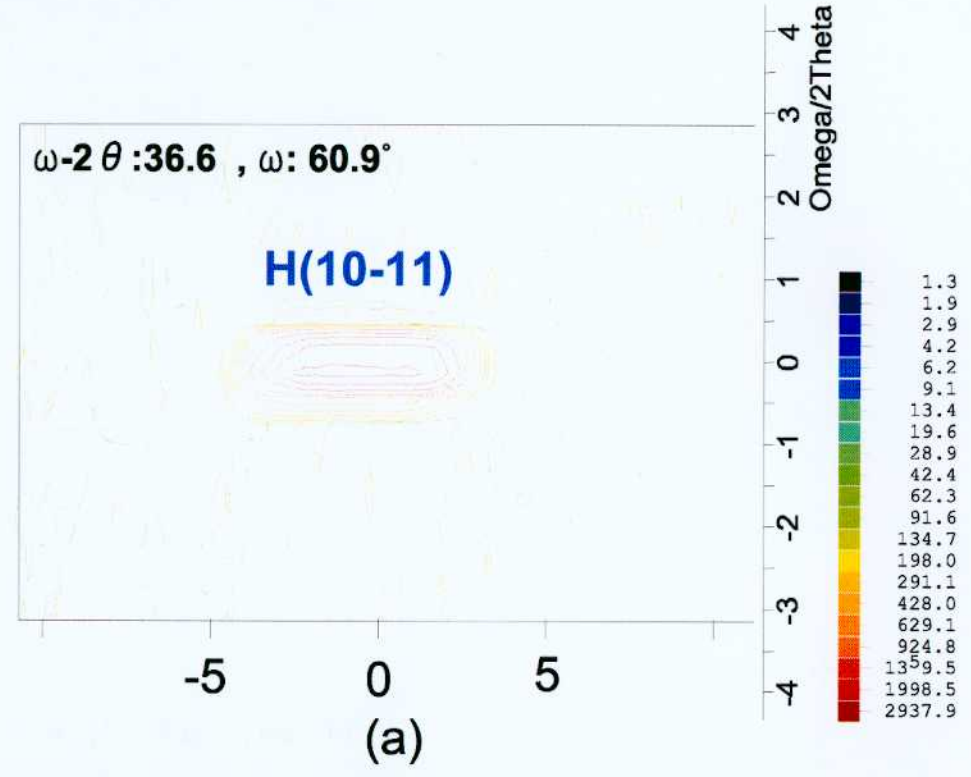

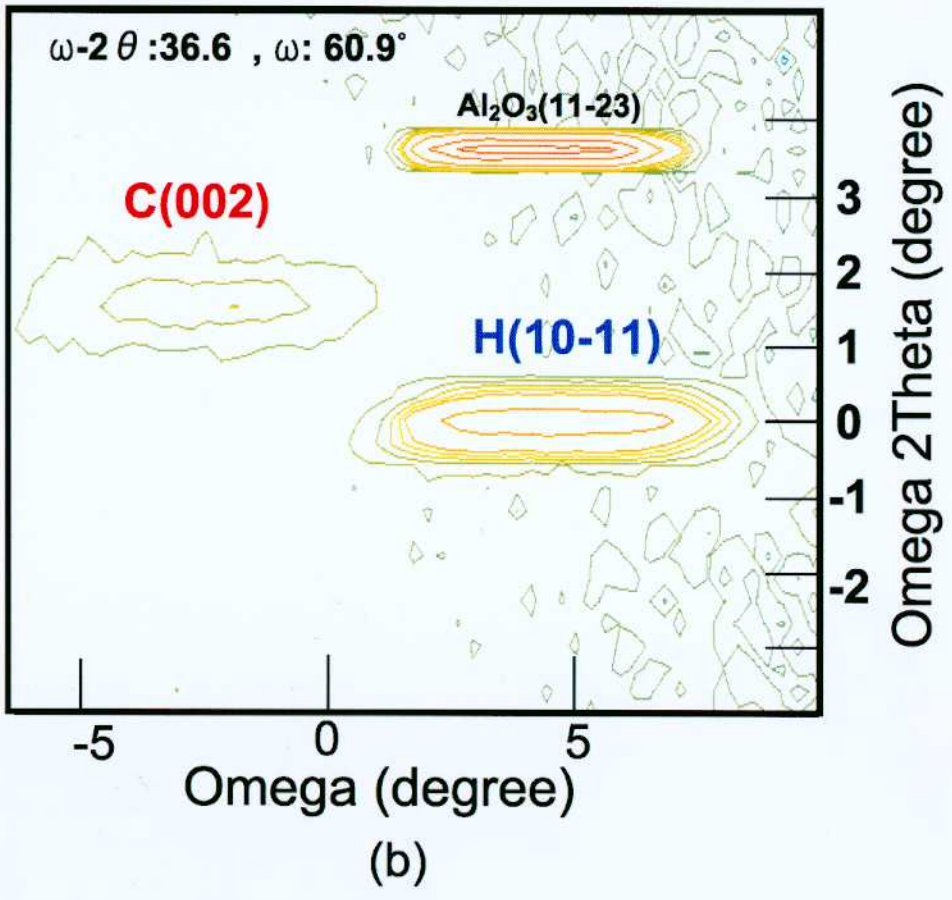

Figure 3-10: Reciprocal lattice mapping of (a) Eu:GaN_Eu390°C and (b) Eu:GaN_Eu450°C

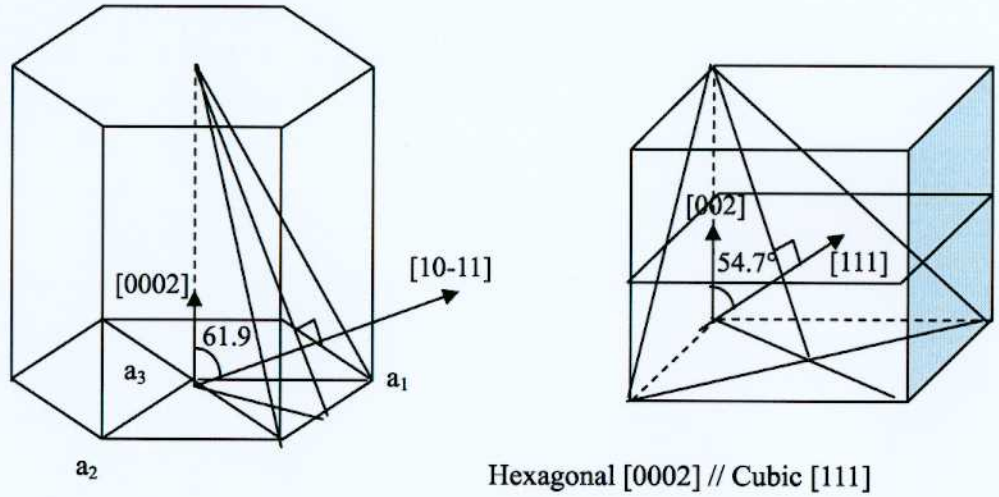

(a)

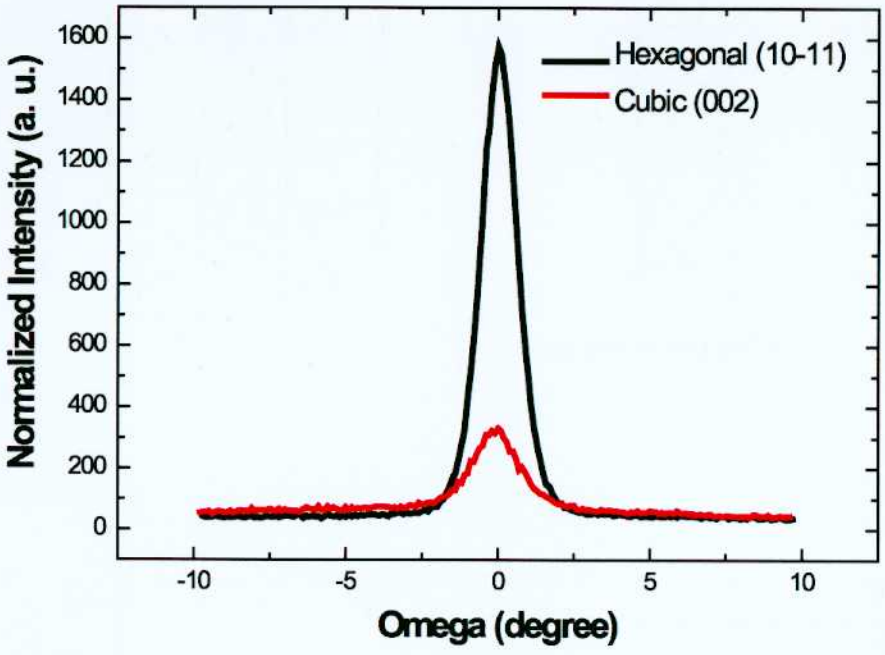

(b)

Figure 3-11: (a) Hexagonal $(10\bar{1}1)$ plane and cubic (002) plane, and (b) ω-scan of both plane

almost same, and has same stacking direction, it is known to be almost impossible to distinguish the cubic phase of GaN and hexagonal phase of GaN on Al_2O_3 (0001) substrate by θ - 2θ method . To compare hexagonal phase and cubic phase, it is generally performed by pole figure or reciprocal lattice mapping. The author carried out reciprocal lattice mapping to detect cubic phase and compared the ω-scan intensity ratio of reflection at (200) plane of cubic GaN with the reflection at $(10\bar{1}1)$ of hexagonal GaN. Fig. 3-10 show reciprocal lattice mapping of Eu:GaN_Eu390 C and Eu:GaN_Eu450 C. For Eu:GaN_Eu390 C, which show only hexagonal spotty pattern on RHEED observation, only $(10\bar{1}1)$ reflection of hexagonal phase of GaN was observed. Conversely, in Eu:GaN_Eu450 C, besides $(10\bar{1}1)$ reflection of hexagonal phase GaN, (002) reflection of cubic phase GaN became comparable. This introduction of cubic phase of GaN shows consistent result with previous RHEED and TEM results. To compare the ratio of cubic and hexagonal phase of GaN in Eu:GaN_Eu450 C, the integral intensity of (002) reflection of cubic GaN which is 54.7° tilted with that of (111) reflection of cubic GaN and $(10\bar{1}1)$ reflection that is 61.9° tilted to (0002) plane of hexagonal GaN as shown in Fig. 3-11 (a), were collected and the ratio was calculated to be 1 / 4 as shown in Fig. 3-11 (b).

Together with the results of RHEED and TEM observation, the strain caused by Eu doping was considered to be relaxed rather by introduction of cubic phase through stacking fault than by broadening the lattice constant in Eu:GaN_Eu450 C. However, in Eu:GaN_Eu500°C, obvious phase separation into EuN and GaN was observed and considered to be strain relaxation mechanism.

3.1.4 Incorporation site and local structure around Eu ion in Eu doped GaN studied by RBS/C and EXAFS analysis.

RBS/C measurements were performed at room temperature with a 2 MeV He ion beam at The Institute of Physical and Chemical Research (RIKEN) on the sample grown at the Eu cell temperature of 390°C, 450°C, and 500°C. The He ion beam was collimated to give divergence less than 0.076°. The beam current and size were about 1.5 nA and 1mm in diameter, respectively. The backscattered He ions were measured with a surface-barrier Si detector placed at an angle of 160° with respect to the incident beam. The sample was mounted on a three-axes goniometer and channeling angular profiles were obtained for the <0001> channel. Eu concentrations in GaN was estimated from random RBS spectra and analyzed to be 0.1 at.%, 2 at.%, and 16 at.% for Eu:GaN_Eu390°C, Eu450°C, and Eu500°C respectively. The random RBS spectra are shown in Fig. 3-12 (a). Fig. 3-12 (b) shows the channeling angular distributions of 0.1 and 2 at.% Eu doped GaN which are normalized to the random yield. For 0.1 at.% doped sample, the angular distribution of Eu signal clearly shows a dip at the same degree with roughly the same value of the full angle at half maximum as that of Ga, indicating that most of Eu atoms are in substitutional sites in GaN. Comparing the depth of the dips between Ga and Eu, it can be estimated that over than 80% of doped Eu atoms are incorporated into substitutional lattice site and thee rest of Eu atoms may be incorporated into random site or interstitial site. For 2 at.% Eu doped GaN, the depth of Ga dip itself is very shallow indicating the degradation of crystal

quality and Eu dip depth is almost half of Ga. Satellite peaks which indicate incorporation into lattice site with large displacemented were also observed.

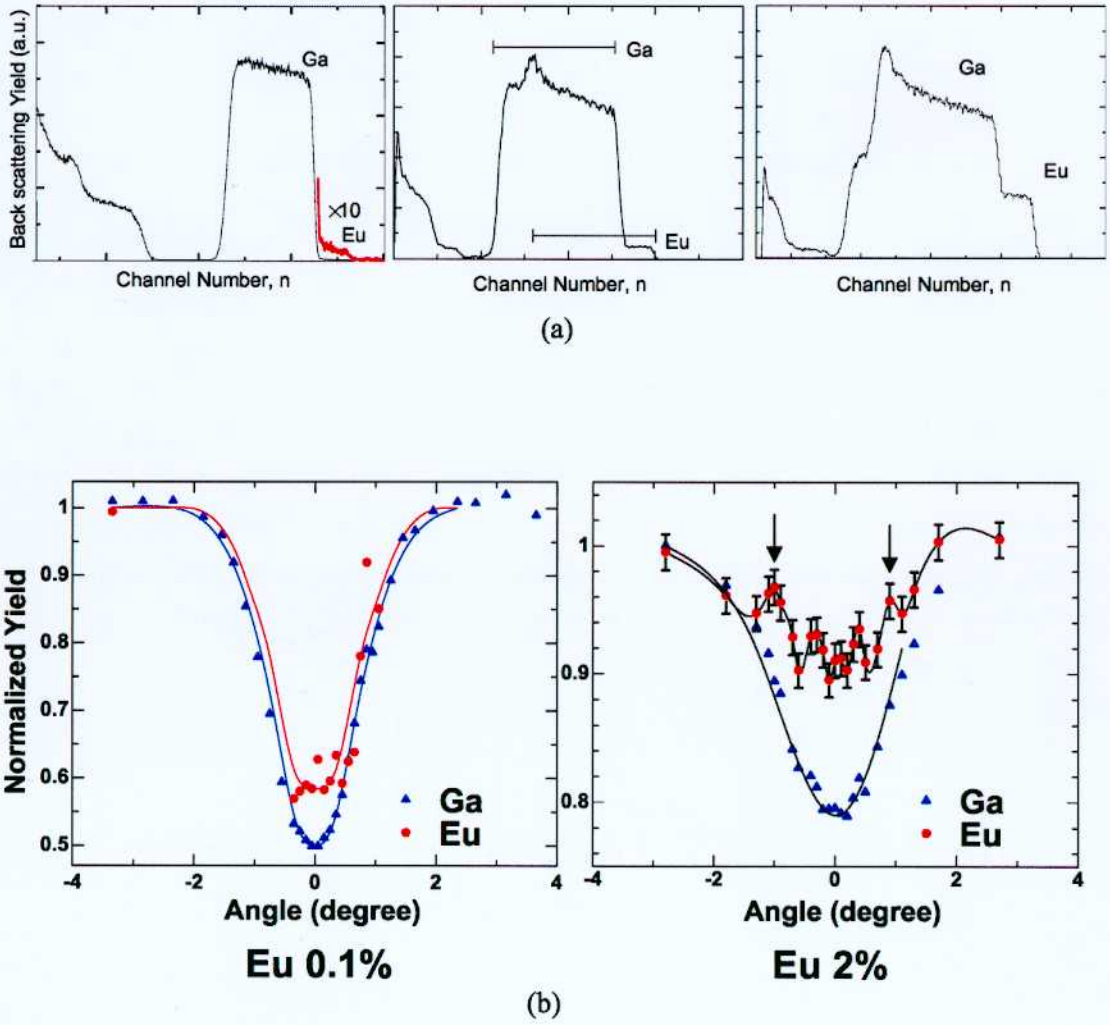

Figure 3-12: (a) The random RBS spectra of Eu:GaN_Eu390°C, 450°C, and 500°C. The concentrations were estimated to be 0.1, 2, and 16 at.% respectively. (b) Normalized channeling angular distributions of 0.1 and 2 at.% Eu doped GaN.

Eu L_{III}-edge EXAFS measurements were carried out for the sample with Eu content of about (A) 0.1 at.%, (B) 2 at.%, (C) 16 at.% in fluorescence mode at beam line 12C in High Energy Accelerator Research Organization (KEK) to study the local structures around Eu atoms. Analysis of the EXAFS data were performed using the general procedure [3-3, 4]. The EXAFS spectra were obtained in fluorescence-detection mode at room temperature. Fourier filtering technique was applied to the first nearest neighbor peak in Fourier transform and the extracted $k^3\chi(k)$ on the shell is curve-fitted using the parameters calculated with FEFF8[3-5] program. The bond lengths, coordination numbers, and Debye-Waller factor were used as fitting parameters to yield optimum values.

Fig. 3-13 (a) shows Eu L_{III}-edge EXAFS spectra of sample (A), (B), and (C). The fluorescence intensity is roughly proportional to the Eu content.The EXAFS function $k^3\chi(k)$ with the k weighting value of 3 was extracted from the L_{III}-edgy fluorescence spectrum and depicted in Fig. 3-13 (b). Upper two spectra in Fig. 3-13 (b) have a similar structure. On the other hand, the lowest spectrum is clearly different from others. The Fourier transformed $k^3\chi(k)$ spectra for (A), (B), and (C) are shown in Fig. 3-13 (c). The relatively large peaks at about 1.6 - 2.5Å and about 2.7 - 3.7Å are attributed to the first and second nearest neighbor atoms, respectively for all samples. Fourier filtering was carried on the range from 1.68 to 2.52Å and from 2.63 to 3.63Å for first and second nearest neighbor atoms, respectively, in sample (A), from 1.55 to 2.38Å and 2.63 to 3.63Å in sample (B), and from 1.55 to 2.38Å and 2.70 to 3.80Å in sample (C). In order to analyze the EXAFS spectra, parameter fitting was conducted with theoretically calculated spectra using the FEFF8 program, which derives the scattering potentials and phase shifts by ab initio calculation. The fitting parameters at optimum fit are shown in Table 3-II.

The analytical results show that most of Eu atoms make bonds with nitrogen with two different bond lengths (2.3, 2.5 Å), and total coordination number of nitrogen is nearly four for all samples. These reveal that most of Eu atoms are incorporated into Ga lattice sites. For the second nearest neighboring atom, the existence of Eu in addition to Ga was suggested. The atomic ratios in second nearest neighbor atoms represent the content of the mixed crystal if the constituent atoms were randomly distributed. The obtained value of the Eu content determined by EXAFS for sample (B) is 2 at.%. This value roughly coincides with that determined by RBS, i.e. Eu ions are almost uniformly distributed on entire film. On the other hand, analyzed Eu content for sample (C) is about 35 at.% and this value is certainly different from the result of RBS (16 at.%). The larger value of Eu content obtained by EXAFS compared with that by RBS means an occurrence of phase separation of EuN from GaN. These results are consistent with the results of XRD.

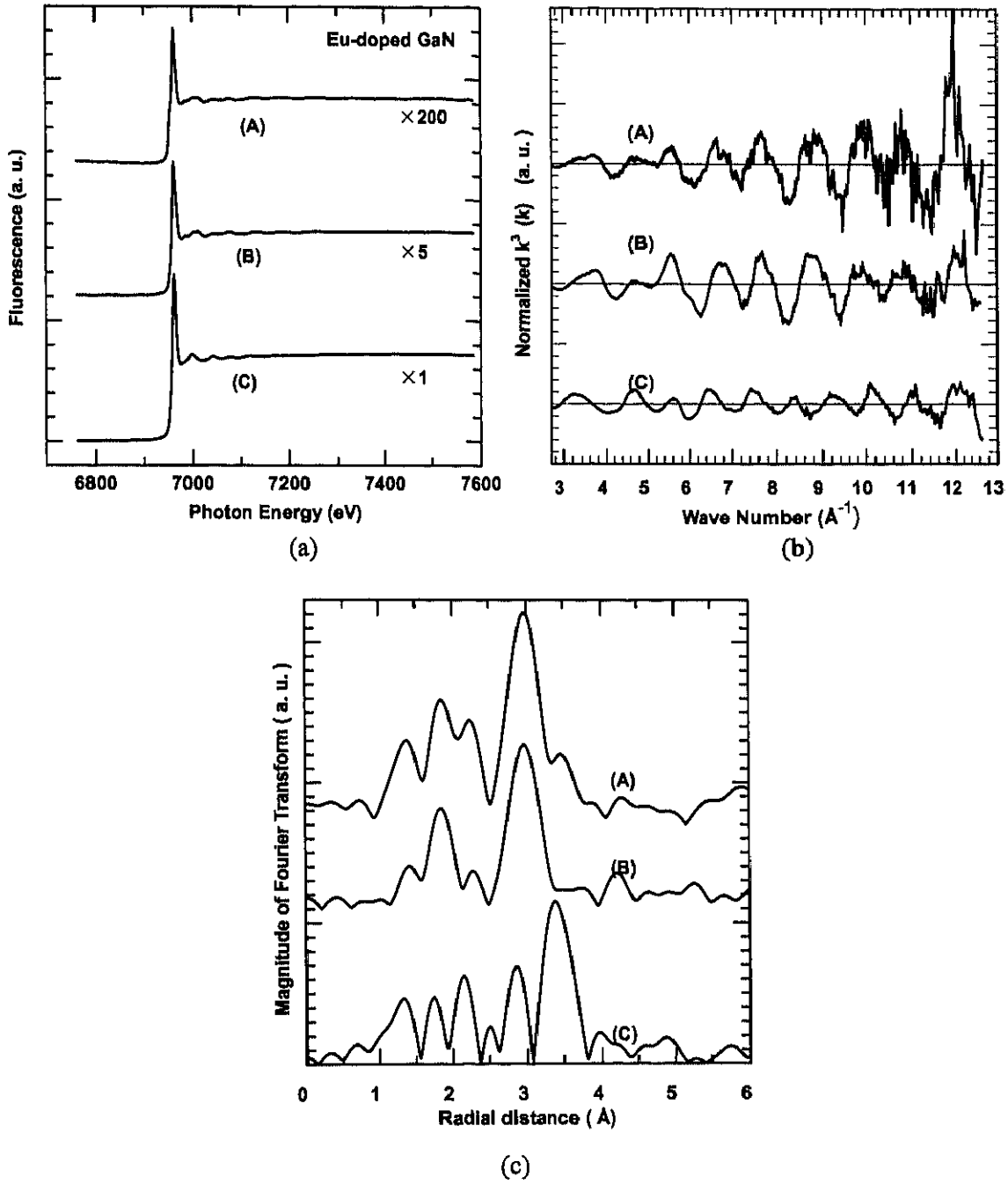

Figure 3-13: (a) Eu L_{III}-edge EXFAS spectra of Eu-doped GaN with the Eu content of (A) 0.1%, (B) 2.2% and (C) 16.6%. (b) Normalized k^3 (k) EXFAS oscillations of (A), (B), and (C). (c) Fourier transform of the k^3-weighed EXFAS oscillation of (A), (B), and (C).

Table 3-II: Analytical results of EXAFS from Eu-doped GaN.

sample	parameter	1st neighbor atom		2nd neighbor atom	
(A) Eu: 0.1%		N		Ga	
	C. N.	1.4	1.8	11.2	
	R (Å)	2.3	2.5	3.4	
(B) Eu: 2 at.%		N		Ga	Eu
	C. N.	2.8	0.8	11.1	0.2
	C. N. ratio			98%	2%
	R(Å)	2.3	2.5	3.3	3.3
(C) Eu: 16 at.%		N		Ga	Eu
	C. N.	0.2	3.0	5.4	2.9
	C. N. ratio			65%	35%
	R(Å)	2.3	2.4	3.3	3.6

3.2 Optical properties of Eu doped GaN.

3.2.1 Luminescence properties measured by PL.

Fig. 3-14 (a) shows PL spectra of (A) undoped GaN and Eu-doped GaN with Eu cell temperature of (B) 390°C, (C) 430°C, (D) 450°C, (E) 480°C, and (F) 500°C. Near band-edge emission of GaN was observed together with red-emission at 622 nm, which can be assigned as $^5D_0$-$^7F_2$ transition[3-6] of Eu^{3+}, for sample (B) and (C). For samples (D), (E), and (F), a red-emission at 622nm was observed without the band edge emission of GaN. PL intensities at 622nm versus various Eu concentrations are plotted in Fig. 3-14 (b). It shows linear increase up to culmination at which Eu concentration is 2 at.%, while further higher Eu doping of over 2 at.% causes abrupt luminescence quenching and shows exponential decay. To improve the emission efficiency, it is important to clarify the cause of the quenching of the luminescence intensity. Intrinsically, alloys formed with component of the host matrix-in this case EuN from GaN-generally known to evoke luminescence quenching, either by increasing ion-ion interactions between rare earth ions or by forming rare-earth compounds that are not optically active. For those reason, concentration quenching of Eu related luminescence in Eu heavily doped GaN may be distributed by a formation of EuN from GaN compounds as detected in XRD and EXAFS measurement.

The temperature dependence of red 622nm emission of 2at.% Eu doped GaN which showed the strongest red emission intensity is shown in Fig. 3-15. At temperature lower than 140K, the PL intensity is almost constant. Above 140K, the photoluminescence intensity relatively strongly quenched but at room temperature it still remains about 25% of its low temperature intensity. Generally such change of temperature results in the decrease of PL intensity of band edge emission GaN or GaAs by

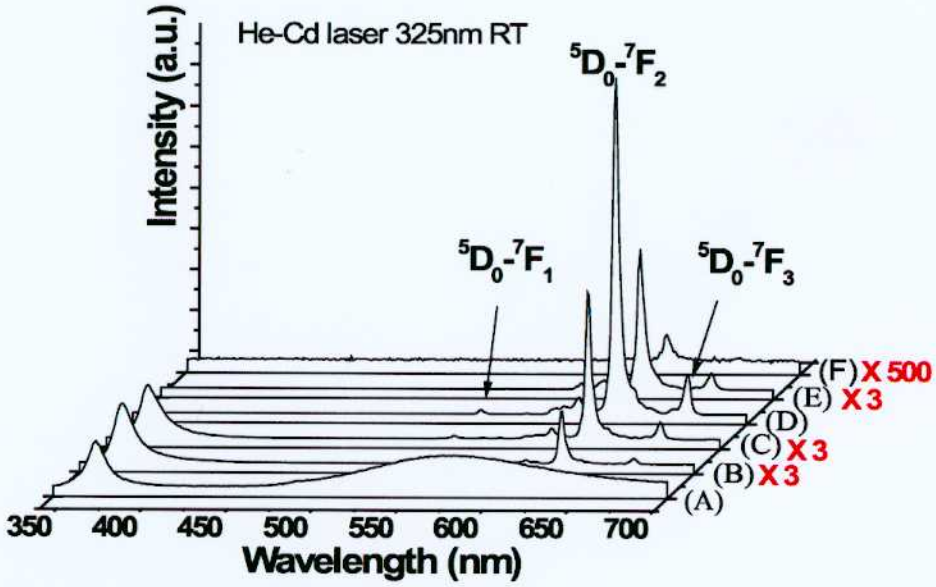

(a)

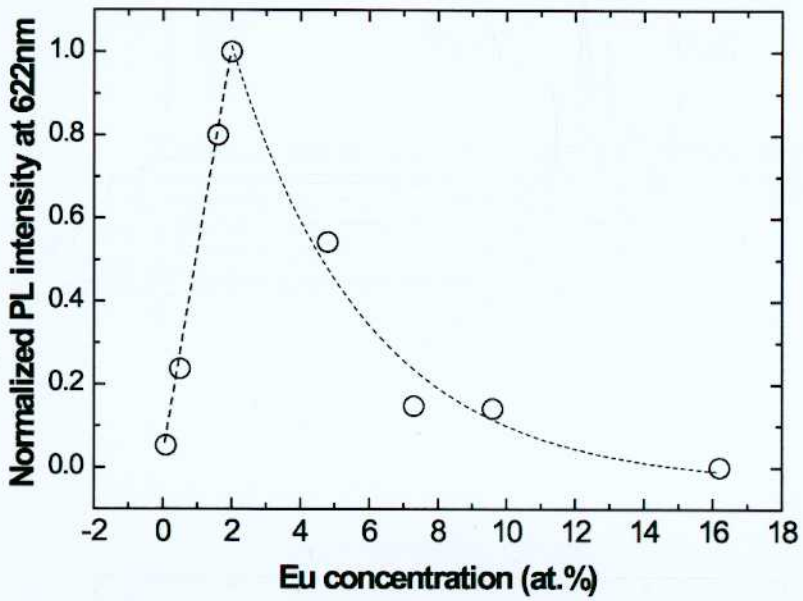

(b)

Figure 3-14: (a)PL spectra of (A) undoped GaN and Eu-doped GaN with Eu cell temperature of (B) 390°C, (C) 430°C, (D) 450°C, (E) 480°C, and (F) 500°C. (b) PL intensities at 622nm versus various Eu concentrations.

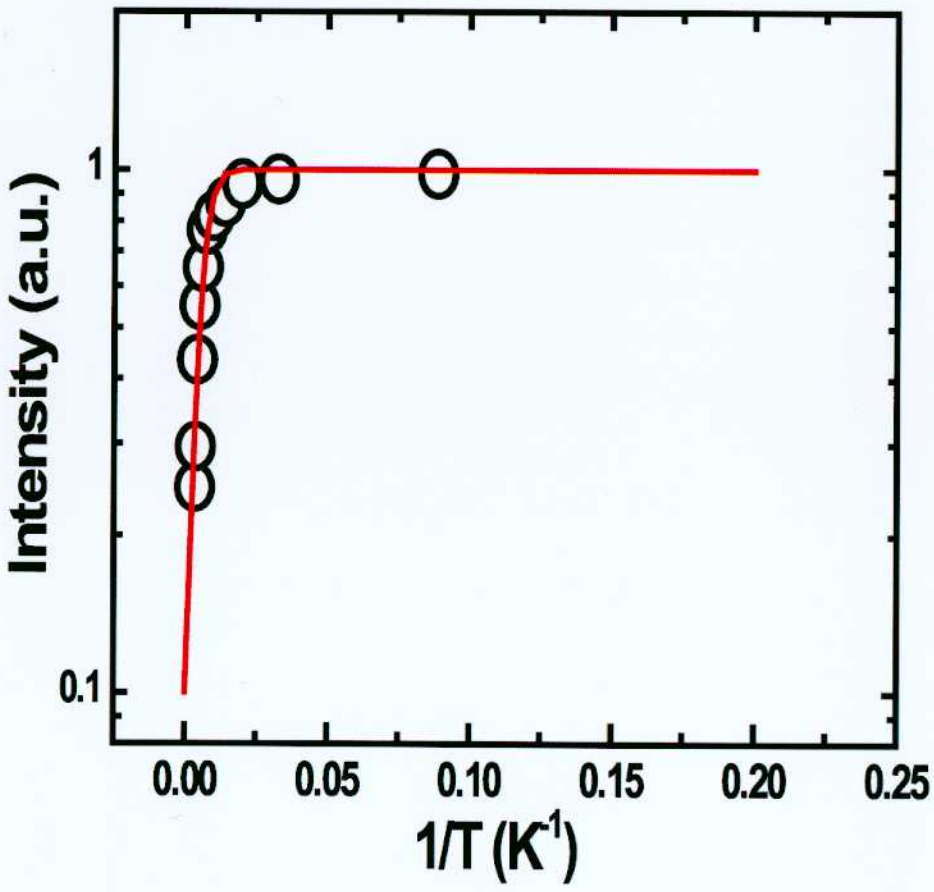

Figure 3-15: The Arrhenius plots of the PL intensity of 2 at.% Eu:GaN. It fits well with the exponential equation with activation energy of 39meV (solid line).

a factor of two orders[3-7]. It is also known that the decays in luminescence intensities from RE in other narrow gap materials such as Er in Si or Yb in InP defend on temperature by a factor of two orders or more[3-8, 9, 10, 11, 12]. This results show that the emission intensity of Eu doped GaN is extremely stable with temperature variation. An exponential model by the equation:

$$\frac{I(T)}{I_0} = \frac{1}{1 + p_1 \cdot exp(-\frac{E_1}{k \cdot T})} \qquad \text{(Eq. 3-1)}$$

is performed and fits well with the parameter value E_1 as 39meV, and p_1 as 9.4 as shown solid red line in Fig. 3-15. Here,E_1 is the activation energy of thermal quenching and p_1 is 'frequency factor' which represents the integral of probability for the change of electron state at certain frequency of excited state. Such a value of activation energy is much smaller than that observed in Er doped Si and Yb doped InP- 0.15 eV in both case[3-8, 9, 10, 11, 12]. The thermal quenching of those materials are reasonably analyzed to be mainly dominated by energy back-transfer, and the observed activation energy of thermal quenching is coincides with the value of the energy difference between the bound exciton recombination and the 4f-shell luminescence energies as shown in Fig. 3-16 (a). For Eu doped GaN, however, the energy difference between 4f-shell transition of Eu^{3+} ion and the exciton recombination is far larger (~1eV) than the observed activation energy of thermal quenching (39meV). Thus, energy back-transfer does not seem to be reason for thermal quenching. The plausible reason for the thermal quenching of Eu doped GaN is considered using hypothetical model of configuration diagram[3-13] as shown in Fig. 3-16 (b). In the figure, the lower parabola is at ground state and upper is at excited state of Eu^{3+} ion. At low temperature, Eu^{3+} ion has a configurational position at r_A. Eu^{3+} ion can make a radiative transition form A to A', then the system will relax to the ground state equilibrium at B. At high temperatures, atomic vibrations can move the atom from a configurational position r_A to position r_C. At C, Eu^{3+} ion can make a non-radiative transition to the ground state. The observed value of activation energy of thermal quenching may indicate the energy value E_1 in figure which makes the transition non radiative.

The author compared the electric dipole $^5D_0$-$^7F_2$ transition strength of Eu^{3+} doped into GaN and other host crystals and shown in Fig. 3-17. The $^5D_0$-$^7F_1$ transition lines of Eu^{3+}, which appear in the high-energy side of the $^5D_0$-$^7F_2$ lines, are due to the parity-allowed magnetic dipole transition, so that the strength of this transition hardly depends on the host crystal. Accordingly, the intensity ratio R of the $^5D_0$-$^7F_2$ transition to the $^5D_0$-$^7F_1$ one is a good measure of the $^5D_0$-$^7F_2$ transition. Calculated R of Eu doped GaN is 12.4 and is relatively large compared with those of most Eu-doped oxide materials[3-14]. We show the comparison with the R values of the Eu doped Y_2O_3 and Y_2O_2S phosphors in Table 3-III. Eu doped Y_2O_3 and Eu doped Y_2O_2S are practical phosphors used for tubular fluorescent lamps and cathode-ray tube displays, respectively, and they are known to have relatively large $^5D_0$-$^7F_2$ transition strengths. Noticeably, R of Eu doped GaN is comparable to that of Eu doped Y_2O_2S and is about twice as large as that of Eu doped Y_2O_3.

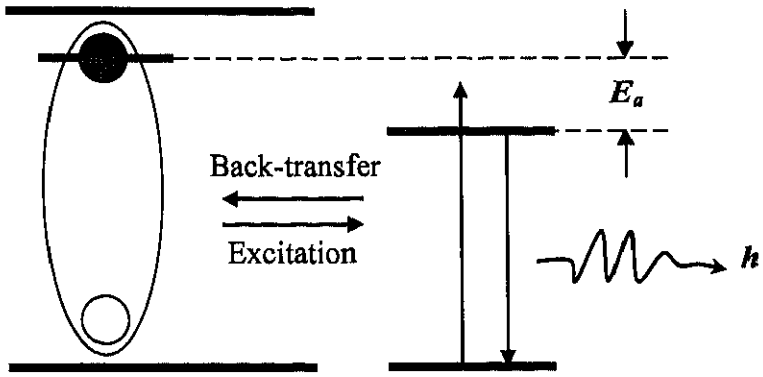

(a)

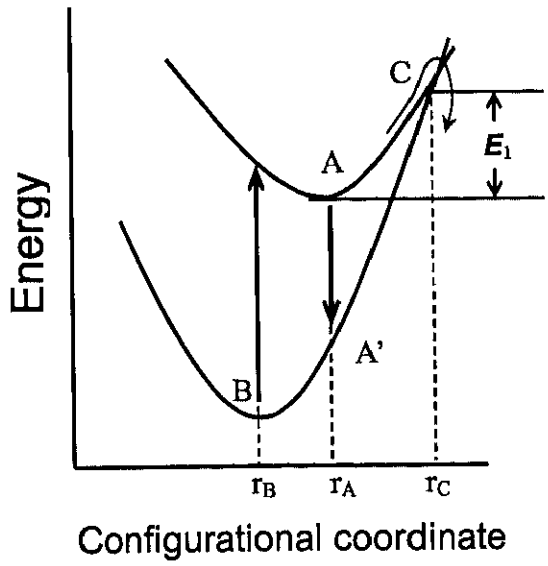

(b)

Figure 3-16: Schematic model of thermal quenching process in (a) Yb doped InP and (b) Eu doped GaN.

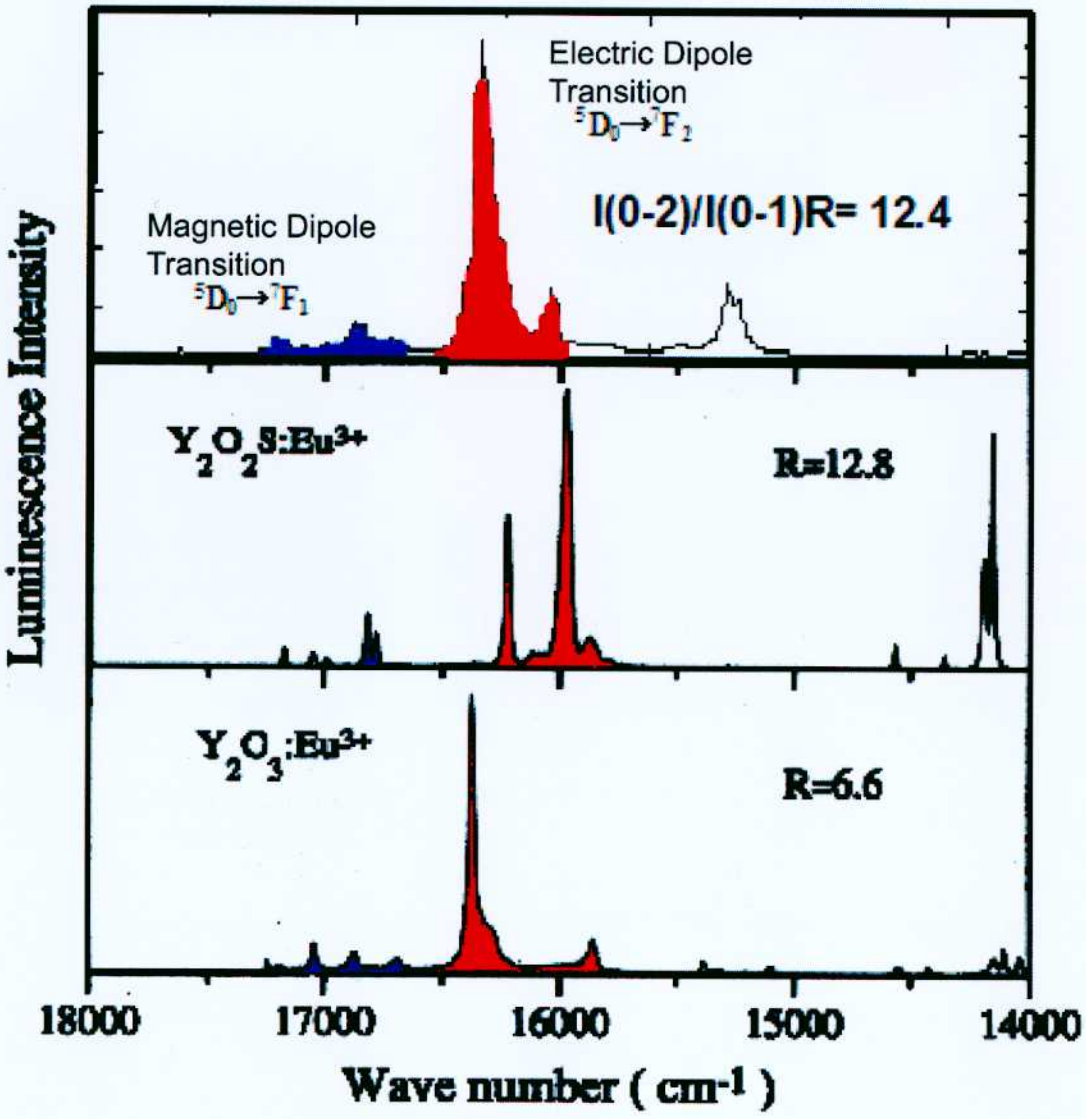

Figure 3-17: The electric dipole $^5D_0$-$^7F_2$ transition strength of Eu^{3+} doped in to GaN compared with magnetic dipole $^5D_0$-$^7F_1$ transition. Those transitions in other host crystals are also shown.

The external emission quantum efficiencies η was also measured by means of photo-calorimetric spectroscopy (PCS), the η of Eu:GaN was estimated to be about to 0.18[3-15]. At that experiments, the η of Eu doped GaN is even higher than that of band edge emission of undoped GaN at room temperature.

Table 3-III: Comparison of the $^5D_0$-$^7F_2$ transition strength among Eu doped GaN and two phosphors

Samples	$R=I(^5D_0\text{-}^7F_2)/I(^5D_0\text{-}^7F_1)$
$Y_2O_2S:Eu^{3+}$	12.8
$Y_2O_3:Eu^{3+}$	6.6
$GaN:Eu^{3+}$	12.4

When it is considered from a practical view, those observed luminescence properties -stability of emission intensity against temperature variation, high external quantum efficiency at RT, etc- are very important, and are revealing strong potential of Eu doped GaN as a material for novel optical applications.

3.2.2 Indirect (carrier mediate) excitation mechanism confirmed by PLE analysis.

Fig. 3-18 show the PLE spectrum of 2 at.% Eu doped GaN measured by monitoring the $^5D_0$-$^7F_2$ luminescence of Eu^{3+} at 622nm. The PLE spectrum exhibits two peaks at wavelength positions of about 364 and 398nm, respectively. The higher-peak position of about 364nm coincides with the band gap energy of GaN. As for the PLE peak at about 400nm, that was observed also in Eu doped GaN grown on the Si substrate by Nyein and co-workers and was ascribed to a transition involving some defect-related trap level [3-16]. On the basis of the PLE spectrum in Fig. 3-18 the excitation of Eu ion can be considered as follow. The electron-hole pair (or exciton) generation by the interband excitation of host GaN preceded and the recombination energy of the electron-hole transferred to Eu ion by means of energy transfer mechanism. The considerable energy transfer mechanism will be explained next subsection. This indirect excitation mechanism of Eu ion doped in GaN is of critical importance when it is practically considered. It is very suggestive property of Eu doped GaN as for an active layer of PN structured LED.

3.2.3 Energy transfer mechanism in Eu doped GaN.

The author argued that the excitation of Eu ion in GaN is occurred by energy transfer preceded by carrier (or electron-hole pair) generation and recombination. Now, the mechanism of how the energy transfer from host GaN to rare earth ion occurs, becomes important issue. The energy transfer mechanisms from host solid matrix to doped RE ion are widely studied and several numbers of models are proposed. Some examples of energy transfer models are shown in Fig. 3-19. Those are (a)

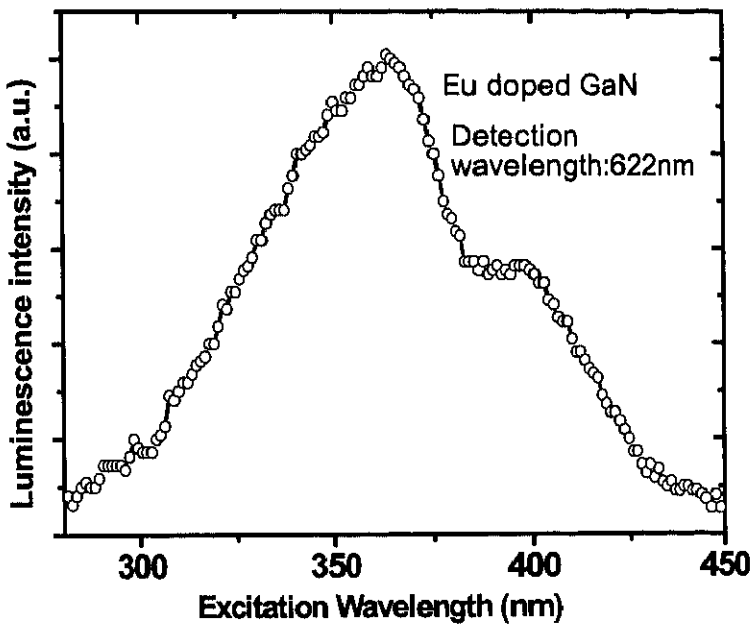

Figure 3-18: PLE spectrum of 2 at.% doped Eu:GaN at room temperature. The luminescence component due to the Eu^{3+} $^5D_0$-$^7F_2$ transition was monitored at about 622nm.

defect related energy transfer model[3-17, 18], (b) resonant energy transfer model[3-19], and (c) bound exciton model[3-20, 21], and shallow center model[3-22] (not shown). Among those models, the author paid attention to the defect related energy transfer model since a trap related peak was observed at around 400nm in PLE measurement as shown in Fig. 3-18. FTIR absorption spectroscopy was hired to detect defect level in Eu doped GaN and the results are shown in Fig. 3-20 (a). The Eu cell temperature of measured samples were in between (I) 390 and (V) 450°C at which the Eu concentration of 0.1at% 2 at.% were determined by RBS measurement. The spectra were normalized by undoped GaN spectrum. It is clear that there exists an absorption peak around 2962cm^{-1}(0.37eV) in all five samples. The undoped GaN (not shown) also shows this feature with very weak intensity. At low Eu cell temperature-(I), the absorption peak was weakly introduced. As Eu cell temperature was increased, the peak became stronger but no peak shift was observed. This result indicates that Eu doping introduces or enhances a trap (defect) level of 0.37eV into GaN host, and the intensity of the trap level increase as Eu becomes concentrated. The Fig. 3-20 (b) gives the relationship between the emission intensity of the red luminescence, the intensity of absorption of FTIR, and the inverse temperature of Eu cell. The vapor pressure curve of Eu was also shown for reference. In the doping scope of 0.1 at.%~2.2 at.%, both intensity of PL and FTIR absorption increased with Eu cell temperature by a super-linear factor. The phenomenon indicates that higher Eu concentration introduces stronger trap level and the level plays an important role in energy transfer process.

The room temperature absorption spectrum gives direct evidence for trap level around 0.37eV. As shown in Fig. 3-21, the enlarged part in inset displays that there is a small but clear absorption step around 3.04eV(408.5nm, 0.35eV lower than band gap of GaN host), which roughly coincides with the results of FTIR.

When the transition probability is taken into account, the detected defect label is plausible to be place below the conduction band (donor-like defect) of GaN rather than above the balance band. There is a report on defect level placed 0.3-0.4eV below the conduction band as well and the level is analyzed to be caused by donor like nitrogen vacancy[3-23]. Based on above experimental results, the author suggests a defect related energy transfer model which explains well the mechanism for the energy transfer from GaN to Eu^{3+} ion. A schematic diagram for the energy transfer is illustrated in Fig. 3-22. Eu doping introduces a trap level in GaN band gap at 0.37eV below the conductive band, as described in Fig. 3-22. The trap captures an electron (step a in Fig. 3-22) and this captured electron attracts a hole by Coulomb force, resulting in the formation of abound exciton. The recombination of the bound exciton (step b) transfers energy to rare earth and an electron is excited to $^5D_3$ level since the trap level has similar energy to $^5D_3$ of Eu^{3+} (step c). This energy transfer may occur thorough Auger transition, electron exchange interaction, or dipole-dipole interaction[3-17, 18, 19, 20, 21, 22, 23, 24]. Then carriers on $^5D_3$ will transmit to $^5D_0$ by non-radiative recombination (step d). Then the transition from $^5D_0$ to ^7F_n gives strong red luminescence (step e). Although the defect structure detected by FTIR should be further analyzed and the energy transfer probability should be estimated theoretically,

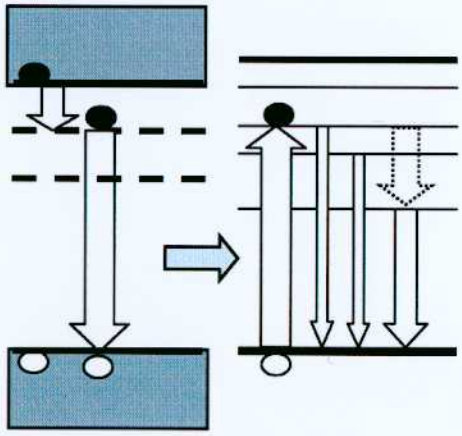

(a) Defect related energy transition model
W. Fuhs et. al., Phys. Rev. B56(1997)9545

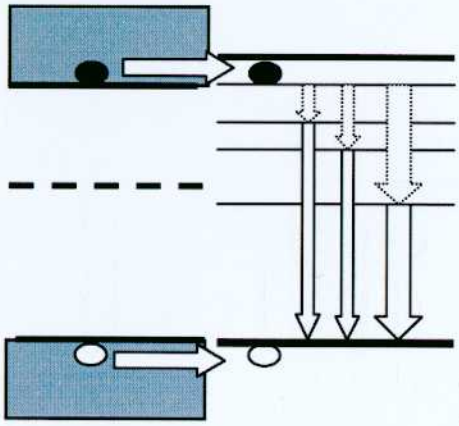

(b) Resonant energy transfer model
H. Kuhne et. al., J. Appl. Phys. 86(1999)896.

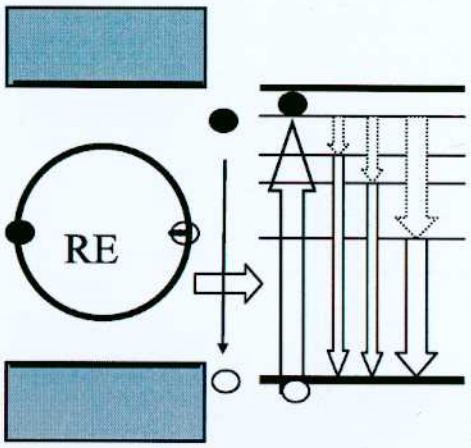

(c) Bound exciton model
J. Palm et. al., Phys. Rev. B54(1996) 17603.

Figure 3-19: Proposed energy transfer models.

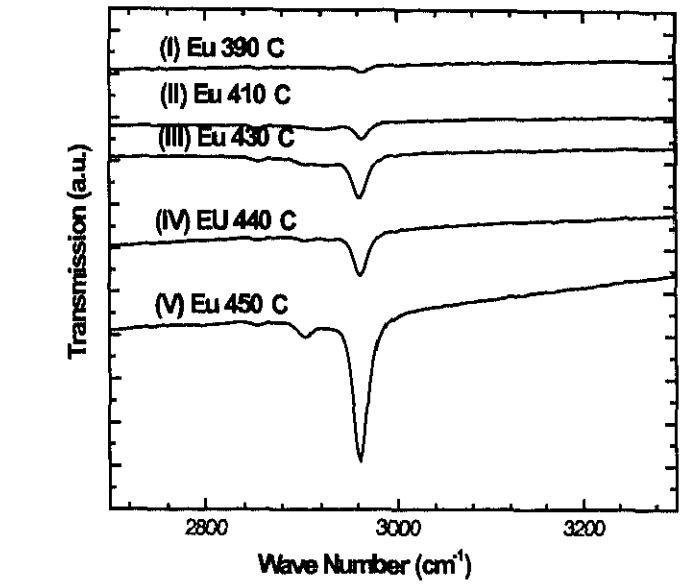

(a)

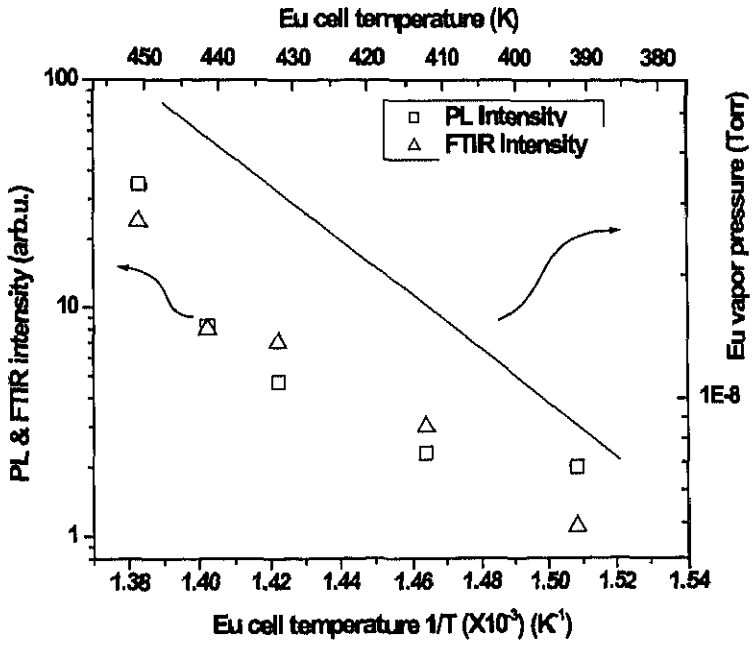

(b)

Figure 3-20: (a) FTIR spectra of Eu doped GaN grown with the Eu cell temperature of (I) 390°C, (II) 410°C, (III) 430°C, (IV) 440°C and (V) 450°C. The transmission spectra are normalized by that of undoped GaN. (b) The Intensity of red luminescence (622nm) and of FTIR absorption peak at 2962cm^{-1} (shown in (a)) vs. inverse temperature of the Eu cell. Vapor pressure curve of Eu is shown for reference.

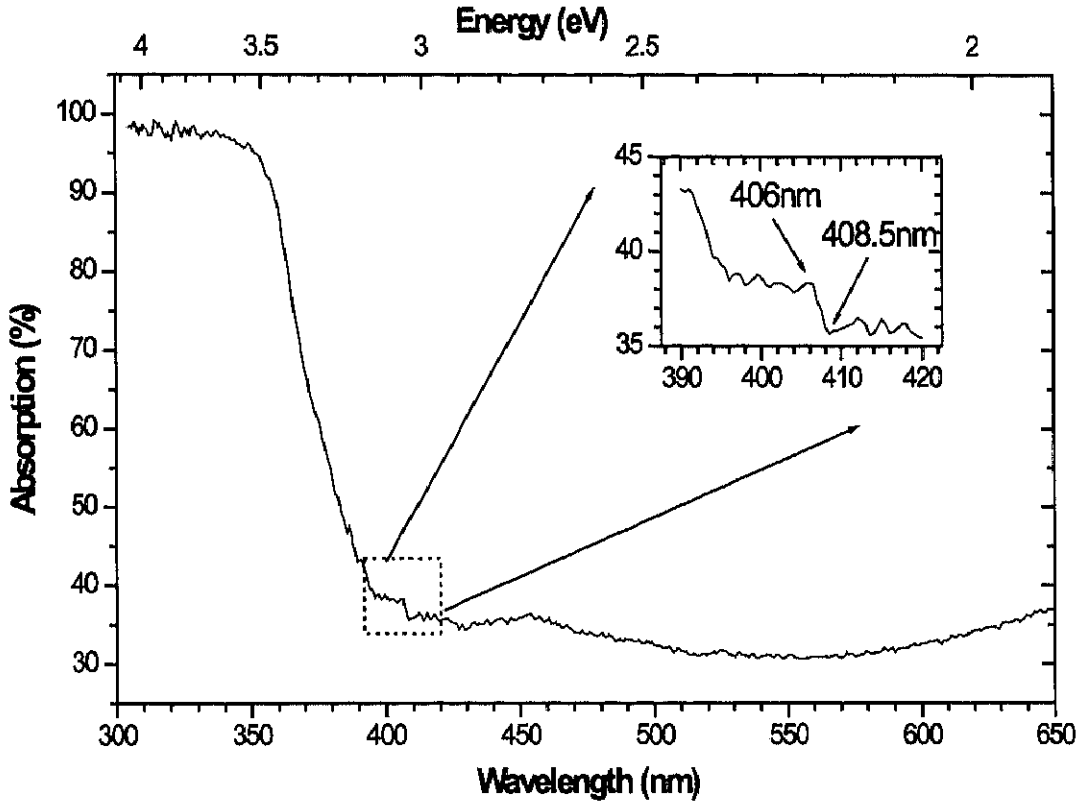

Figure 3-21: Room temperature optical absorption spectrum of 2 at.% Eu doped GaN. The enlarged part shows clear absorption step around 3.04eV.

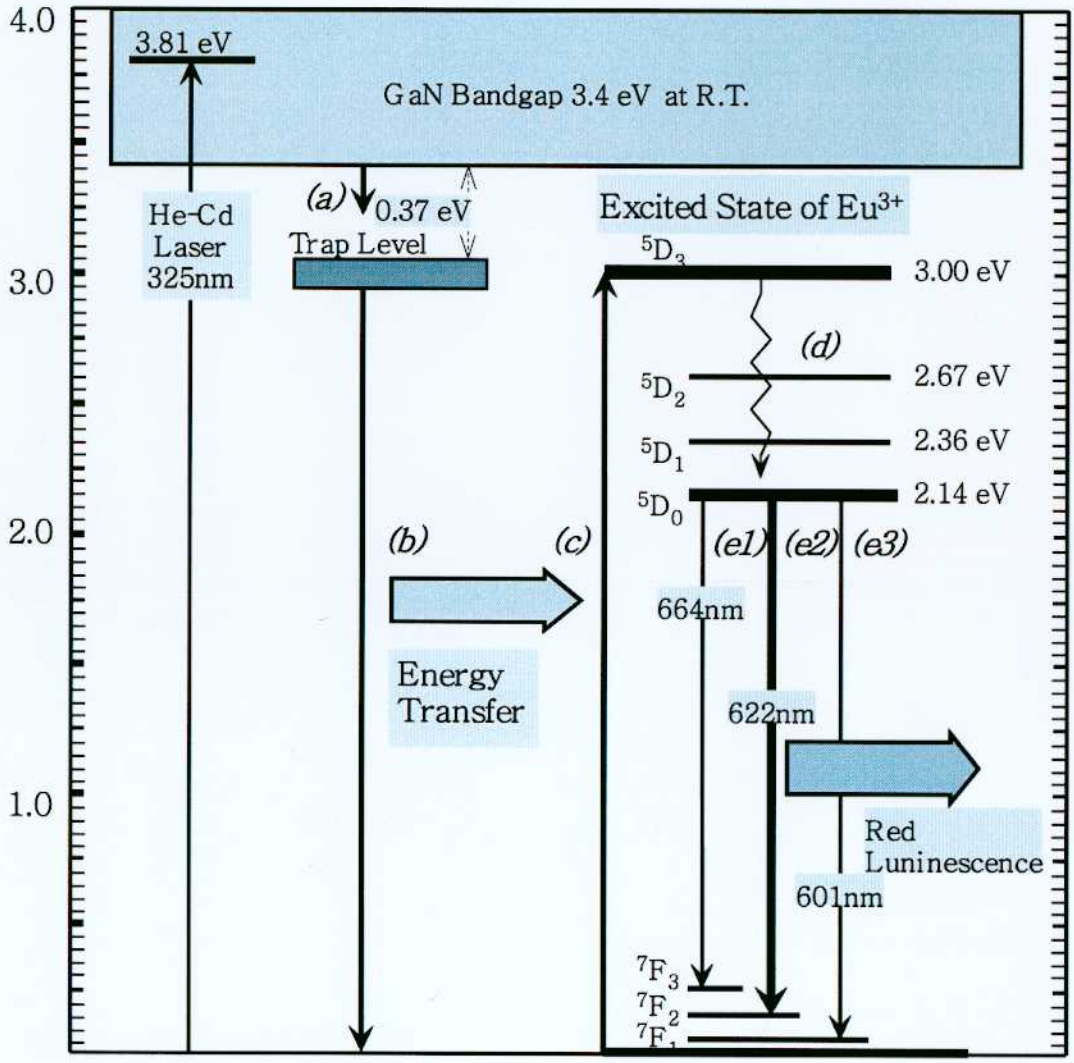

Figure 3-22: Schematic diagram of energy transfer process by defect-related energy transfer in Eu-doped GaN.

defect related energy transfer is more reasonable for the energy transfer mechanism in Eu doped GaN based on our experimental results.

3.2.4 RED electroluminescence (EL) from metal/insulator/semiconductor (MIS) structured LED

MIS diode having an In/Eu doped GaN (0.3 μm)/undoped GaN (0.3 μm) structure was fabricated on n-type silicon (Si)(111) substrates. Fig. 3-23 shows the EL spectrum of the MIS diode operated under a dc biasing about 5 V. The EL spectrum shows red emission with the wavelength at around 622 nm just the same as in the PL spectra. The emission efficiency is low at present. In case of the MIS structure, impact excitation may be dominant for optical emission of impurities, that is, the Eu3+ is excited directly by the collisions with hot electrons. Therefore, the efficiency can be improved by using Eu doped GaN as an active layer material in a pn junction.

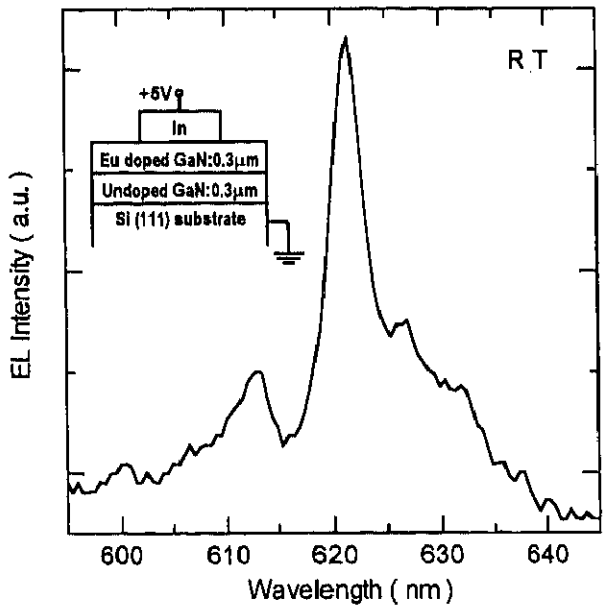

Figure 3-23: EL spectrum of MIS diode

To summarize this chapter, the author showed the structural and optical properties of Eu doped GaN. Single crystalline growth, mixing of Cubic phase, and phase separation into EuN from GaN and GaN were observed for 0.1 at.%, 2 at.%, and 16 at.% Eu doped sample, respectively. The red emission, showed very small temperature-dependency on emission intensity, high emission efficiency, and the carrier-mediate-emission mechanism indicate the potential of Eu doped GaN as material for novel photoelectron devices.

Chapter 3 References

[3-1] http://web.mit.edu/3.091/www/pt/pert5.html

[3-2] H. Jacobs, U. Fink, Zeitschrift fur anorganische und allgemeine Chemie 438, 151 (1978).

[3-3] P. A. Lee, P. H. Citrin, P. Eisenberger, and B. Kincaid, Rev. Mod. Phys. 53, 769 (1981).

[3-4] D. E. Sayers and B. A. Bunker, X-ray Absorption: Principles, Applications, Techniques of EXAFS, SEXAFS, and XANES (Edited by D. C. Koningsberger and R. Prins), Charp. 6. Wiley, Newyork (1988).

[3-5] A. L. Ankudinov, B. Ravel, J. J. Rehr, and S. D. Conradson, Phys. Rev. B58, 7565 (1998)

[3-6] G. H. Dieke, Spectra and Energy Levels of Rare Earth Ions in Crystals, Chapter 13, (John Wiley & Sons, 1968, New York.).

[3-7] M. Leroux, N. Grandjean, B. Beaumont, G. Nataf, F. Semond, J. Massies and P. Gibart, J. Appl. Phys. 86, 3721 (1999).

[3-8] S. Coffa, G. Franzo, F. Priolo, A. Polman and R. Serna, Phys. Rev. B49, 16313 (1994).

[3-9] W. Fuhs, I. Ulber, G. Weiser, M. S. Bresler, O. G. Gusev, A. N. Kuznetsov, V. Kh. Kudoyarova, E. I. Terukov and I. N. Yassievich, Phys. Rev. B56, 9545 (1997).

[3-10] J. Palm, F. Gan, B. Zheng, J. Michel and L. Kimerling, Phys. Rev. B54, 17603 (1996).

[3-11] A. Taguchi, M. Taniguchi and K. Takahei, Appl. Phys. Lett. 60, 965 (1992).

[3-12] A. Taguchi, K. Takahei and Y. Horikoshi, J. Appl. Phys. 76, 7288 (1994).

[3-13] J. I. Pankove, in: Optical Processes in Semiconductors, Chap. 7, Dover Publ., Inc., New York 1971 (p.167).

[3-14] W. C. Nieuwpoort and G. Blasse, Solid State Commun. 4, 227 (1966).

[3-15] T. Maruyama, H. Sasaki, S. Morishima, and K. Akimoto, phys. stat. sol. (b) 216, 619 (1999).

[3-16] E. Nyein, U. Hommerich, J. Heikenfeld, D. S. Lee, J. Steckl, and J. M. Zavada, Appl. Phys. Lett. 82, 1655 (2003).

[3-17] W. Fuhs, I. Ulber, G. Weiser, M. S. Bresler, O. B. Gusev, A. N. Kuznetsov, V. Kh. Kudoyarova, E. I. Terukov, and I. N. Yassievich, Phys. Rev. B56, 9545 (1997).

[3-18] Irina Yassievich, Mikhail Bresler, Oleg Gusev, J Non-Cryst. Sol. 226, 192 (1998).

[3-19] H. Kühne, G. Weiser, E. I. Terukov, A. N. Kusnetsov, and V. Kh. Kudoyarova, J. Appl. Phys. 86, 896 (1999).

[3-20] J. Palm, F. Gan, B. Zheng, B. Michel, and L. C. Kimerling, Phys. Rev. B54, 17603 (1996).

[3-21] I. Tsimperidis, T. Gregorkiewicz, H. H. P. Th. Bekman, C. J. G. M. Langerak, Phys. Rev. Lett. 81, 4748 (1998).

[3-22] T. Gregorkiewicz, J. M. Langer, H. H. P. Th. Bekman, M. S. Bresler, J. Michael and L. C. Kimerling, Phys. Rev. B61, 5369 (2000).

[3-23] T. L. Tansley and R. J. Egan, Phys. Rev. B45, 10942 (1992).

[3-24] A. Kudo and T. SakataA, J. Phys. Chem. 99, 15963 (1995).